Digital Topography Models for Martian Surfaces

Tomasz Stepinski and Ricardo Vilalta

***Abstract*— We propose to use an unsupervised automated classification of topographic features on Mars in order to speed up geomorphic and geologic mapping of the planet. We construct a digital topography model (DTM), a multi-layer grid that stores various kinds of topographical information for every pixel in a site. The method uses a probabilistic clustering algorithm to assign topographically meaningful labels to all pixels in the DTM. The results are displayed as a thematic map of topography. Resultant topographical features are characterized and compared using statistics of their constituent pixels. We demonstrate the usage of our method by classifying and characterizing the topography of a landscape in the Tisia Valles region on Mars. We discuss extensions and further applications of our method.**

***Index Terms*— Digital topography, unsupervised classification, automated extraction of features, landscape characterization, Mars.**

I. Introduction

Mars is at the center of our current solar system exploration efforts. In particular, there are presently three orbiters, remotely collecting information about Martian surface from their orbits. These are, NASA Mars Global Surveyor (MGS), Mars Odyssey Orbiter, and ESA Mars Express. The orbiters gather data that can be divided into three broad categories: imagery data, topography data, and spectral data.

Imagery data has been the first to be collected (starting with Mariner and Viking probes) and it continues to be used as the primary source of information about the Martian surface. A standard mapping technique of photogeologic interpretation of images [1] has been developed to identify the topographic, stratigraphic and tectonic relationship of surface units and to produce geologic maps. However, geologic mapping based on photogeologic interpretation of images is a manual and laborious procedure. Tools for automating the analysis of all types of remotely collected Martian data are lacking.

In this paper we concentrate on a methodology for automating an analysis of Martian topography data. The Martian topography data was gathered by the Mars Orbiter Laser Altimeter (MOLA) instrument [2] aboard the MGS spacecraft. This data was subsequently used to construct [3] global topographic maps of Mars in the form of digital elevation models (DEMs). Our goal is to develop an unsupervised automated method for classification and characterization of Martian topographic features. Fast and objective characterization of Martian topography would alleviate the tedious task of photogeologic interpretation of topographical features from images and would significantly speed up production of geomorphic and geologic maps.

Manuscript received January 20, 2002; revised November 18, 2002.

T. Stepinski is with the Lunar and Planetary Institute, 3600 Bay Area Blvd., Houston, TX 77058, USA (e-mail: tom@lpi.usra.edu)

R. Vilalta is with the Dept. of Computer Science, University of Houston, 4800 Calhoun Rd., Houston, TX 77204, USA (e-mail: vilalta@cs.uh.edu)

In a terrestrial framework, methods for an automated classification of landforms have been developed (see for example [4]) and applied in various contexts. For example, at a large scale, to define topographic provinces [5], or, at a small scale, for use in a soil-landscape study [6]. In this paper we present an approach to an automated landform classification that is primarily intended to be used for production of geomorphic maps of Mars. Central to our approach is the concept of a digital topography model (DTM), an organization of topographical information that enables automated classification and statistical analysis of topographical features on Mars. The DTM is a significant extension of the familiar notion of the DEM. Individual pixels in the DTM carry an array of local and regional topographical information that allows assigning pixels to specific topographic formations. Thus, in our method, an automated recognition of topographical features is achieved on the local level of its constituent pixels by means of a clustering algorithm that groups pixels carrying similar information into classes corresponding to topographic features. Because the classification is achieved at the pixel level, its results can be conveniently visualized by means of a thematic map of topography. In addition, pixel-level classification makes possible the characterization and comparison of different topographical formations using statistical analysis.

The objective of this paper is to describe the concept of a DTM and to demonstrate how it can be used for an unsupervised, automated classification and characterization of Martian landscapes. The concept of a DTM is laid down in Section II and our classification method is described in Section III. The results of applying our method to Tisa Valles, a test site on Mars, are presented in Section IV. A statistical comparison between selected topographic formations identified for Tisa Valles is given in Section V. Section VI contains summary and discussion.

II. Digital Topography Models

A DEM, $\mathcal{E}(x, y)$, is a quantized planar rectangular space where each pixel (labeled by x and y) is assigned an elevation value $\mathcal{E}(x, y) = z(x, y)$. In a DTM, each pixel, $\mathcal{T}(x, y)$, is assigned a list of N values, $\mathcal{T}(x, y) = \{\mathcal{T}_1(x, y), \ldots, \mathcal{T}_l(x, y), \ldots, \mathcal{T}_N(x, y)\}$, that includes, but is not limited to, an elevation. The DTM, viewed as a data structure, is a 3-D array consisting of N layers with each layer holding a different topographic information organized in a 2-D grid.

By construction, the DTM is somewhat analogous to the concept of a multispectral image, but it pertains to topographical rather than imagery data. Unlike a multispectral image (see, for example [7]), where every layer contains an intensity of light measured at a particular part of a spectrum, the layers in the DTM contain variables with different physical meanings.

In this paper we construct the DTM with $N = 6$ layers. The first layer of the DTM, $\mathcal{T}_1(x, y)$, contains an elevation field, $z(x, y)$. We artificially modify the original elevation field using the so-called "flooding" algorithm. It identifies all enclosed depressions (pits) in $z(x, y)$ and raises their elevation to the level of the lowest pour point around their edges thus producing a flooded elevation field $z_f(x, y) \geq z(x, y)$. A field $\delta(x, y) = z_f(x, y) - z(x, y)$ has non-zero values only for pixels located inside depressions. Large values of δ flag pixels located deep inside depressions. In the context of Martian topography, pixels located inside craters can be identified using the values of δ. The second layer of the DTM, $\mathcal{T}_2(x, y)$, holds the values of $\delta(x, y)$.

For a given pixel (x_0, y_0) we calculate the set of slopes between it and the eight of its nearest neighboring pixels using the original elevation field. The pixel's slope, $s(x_0, y_0)$, is the largest slope in this set. Pixels at the boundaries of the DTM, where slope cannot be determined, are assigned the value of -1. The third layer of the DTM, $\mathcal{T}_3(x, y)$, holds the values of $s(x, y)$. A different field of slopes, $s_f(x, y)$, is associated with the flooded elevation field and it constitutes the fourth layer of the DTM, $\mathcal{T}_4(x, y) = s_f(x, y)$. We also store pixels' slope directions, but this information is not assigned to any layer.

A contributing area, $a(x_0, y_0)$ is the total number of pixels "draining" through a given pixel (x_0, y_0). The term draining is used here as a metaphor for connectivity between different pixels in a landscape. A pixel counts toward the contributing area of (x_0, y_0) if there is a chain of slope directions linking it to (x_0, y_0). In landscapes that are indeed subjected to rainfall, a contributing area is tantamount to a drainage area. Small values of a flag pixels located on topographic peaks, ridges, and divides. Large values of a flag potential streams. The field of contributing areas calculated for the flooded elevation field is denoted by $a_f(x, y)$. The fifth and sixth layers of the DTM, $\mathcal{T}_5(x, y)$ and $\mathcal{T}_6(x, y)$, hold values of $a(x, y)$ and $a_f(x, y)$, respectively.

The values for $\mathcal{T}_1$ are taken directly from a DEM. The values for the layers $\mathcal{T}_2$ to $\mathcal{T}_6$ are calculated using a software suite TARDEM [8]. Note that a value assigned to a pixel in layers $\mathcal{T}_2$, $\mathcal{T}_5$, and $\mathcal{T}_6$ depends on information gathered from a neighborhood (of varying size) of this pixel. This makes pixels "aware" of their topographic context.

III. Classification of pixels in the DTM

Each pixel (x_0, y_0) in the DTM holds a 6-D pixel vector, $\mathcal{T}(x_0, y_0) = \{\mathcal{T}_1(x_0, y_0), \ldots, \mathcal{T}_6(x_0, y_0)\}$, that we call a descriptor because it contains information capable of determining the topographical context of that pixel. Our task is to perform an unsupervised classification of all pixels in the DTM based on similarity of the values of their descriptors. Two pixels are similar if $\mathcal{T}(x_1, y_1)$ and $\mathcal{T}(x_2, y_2)$ are close in the sense of Euclidian metric. We apply a clustering algorithm over the DTM that produces as output a set of k classes, $\mathcal{C}_k = \{c_1, c_2, \ldots, c_k\}$, where each class c_i contains a list of pixels that are similar to each other. The set of classes is mutually exclusive and exhaustive. Because similar pixels correspond to similar topographical context, such classification can be used to produce a thematic map of topography, $\mathcal{M}(x, y)$, a 2-D array of the same dimensions as the planar dimensions of $\mathcal{T}$. Each pixel in $\mathcal{M}$ is assigned a label c_i of a class to which a corresponding pixel in $\mathcal{T}$ belongs.

We cluster the DTM using a probabilistic clustering algorithm working under the Bayesian framework. In principle, a pixel vector $\mathcal{T}(x_0, y_0)$ is assigned to the cluster c_i exhibiting highest posterior probability, $P(c_i|\mathcal{T}(x_0, y_0)) > P(c_l|\mathcal{T}(x_0, y_0)$, $l = 1 \ldots k$, $l \neq i$. In practice, by virtue of Bayes' theorem, a class c_i is assigned to a vector $\mathcal{T}(x_0, y_0)$ if it maximizes $P(\mathcal{T}(x_0, y_0)|c_i)P(c_i)$. Estimation of parameters characterizing the likelihood function, $P(\mathcal{T}(x_0, y_0)|c_i)$, and the prior probability, $P(c_i)$, are performed using the Expectation Maximization (EM) technique [9]. The number of classes is calculated using cross-validation [10]. Because a non-trivial DTM contains a large amount of data, a direct clustering via the probabilistic technique is computationally expensive. To alleviate this problem we have devised the following procedure. First, we sample the DTM to create a smaller, initial dataset of pixels. This initial dataset is clustered into $\mathcal{C}_k$ using the probabilistic technique. The remaining pixels are classified into $\mathcal{C}_k$ using a decision tree learning algorithm [11] constructed on the basis of the initial dataset.

IV. Application to Tisia Valles region

To demonstrate the utility of the DTM for producing a thematic map of topography on Mars, we have chosen a specific region around Tisia Valles. Fig. 2A. shows a shaded relief of this site rendered using digital elevation data. The center of the site is located at 46.13°E, 11.83°S. The terrain shown is approximately 215 km west to east and 192 km south to north. We have selected this site because it encompasses, in a relatively small area, all topographic features (craters, channels, ridges, and plains) that are of interest in studying ancient Martian surface.

We have used digital elevation data from the MOLA Mission Experiment Gridded Data Record (MEGD) [3] to construct a DEM covering the terrain depicted on Fig. 2A. The DEM has a resolution of 1/128 degrees, its dimensions are 385 rows and 424 columns. The DTM is constructed as described in Section II. The elevation range is 1810 to 3580 meters. Eight equispaced topographic contours shown on Fig. 2A span that range of elevation values. Flooding adjustment affects 31% of the pixels and the maximum flood is 947 meters. The largest value of a is 2005 pixels, slightly more than 1% of the total number of pixels. This indicates that an unadjusted elevation field lacks regional connectivity and breaks into a large number of small "basins." However, the largest value of a_f is 68,625 pixels covering over 40% of the landscape area. Thus flooding adjusts the elevation field so it becomes regionally connected. Fig. 1. shows a visual representation for four out of six layers of the DTM. The leftmost panel on Fig. 1 represents $\mathcal{T}_1$ and visualizes a topography of the Tisia Valles site. Examination of other panels on Fig. 1. reveals that $\mathcal{T}_2$ identifies craters, $\mathcal{T}_3$ identifies sloped walls of craters, and $\mathcal{T}_6$ identifies ridges and channels.

Because variables stored in different layers of the DTM have different physical meaning and different range of values, we

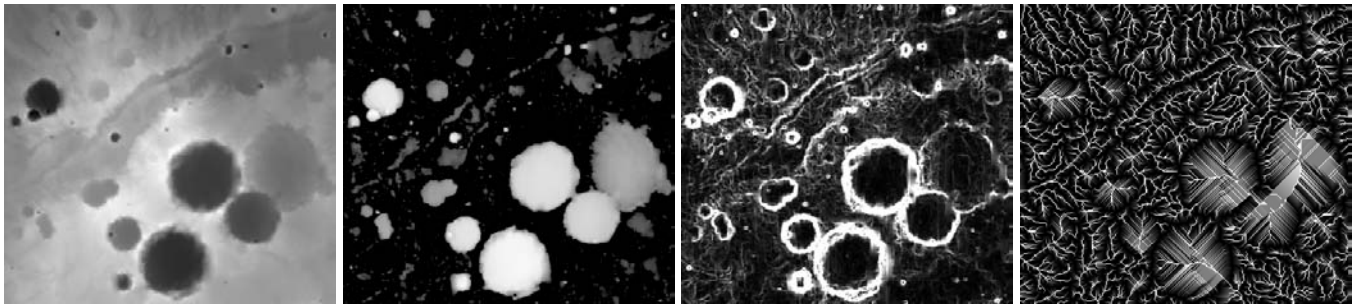

Fig. 1. Visual representation of topographical data layers constructed for Tisia Valles region on Mars. The layers are, from left to right, an elevation ($\mathcal{T}$), the flooding adjustment ($\mathcal{T}_2$), slopes ($\mathcal{T}_3$), and the contributing area for flooded elevation field ($\mathcal{T}_6$). The white to black gradient corresponds to highest to lowest values of variables.

have normalized each variable so its values are in the range $(0, 1)$. This normalization causes all variables to contribute equally to the "distance" between different pixels. The 40,000 pixels were randomly chosen from the normalized DTM to create an initial dataset. We have assured an uniform sampling to obtain an unbiased representation of all, even rare landscape features. Our clustering algorithm has classified these 40,000 pixels into 10 classes. The remaining pixels were classified into those 10 classes using a decision tree algorithm. We assess separations between the final classes by calculating a matrix of inter-class distances expressed in terms class sizes. We have found that for the vast majority of class pairs the inter-class distances are > 1 indicating strong separation. Thus, our final set of classes constitutes a meaningful classification.

Fig. 2B. is a thematic map of topography of the Tisia Valles region constructed on the basis of our classification. Pixel class membership is indicated by different shades of gray. After reviewing statistical properties of descriptors in each class we gave physical interpretations to these classes. The legend on Fig. 2B. summarizes our interpretation. We have divided the 10 classes into 4 groups, craters (**C**), inter-crater plateau (**P**), ridges (**R**), and channels (**CH**).

The majority of pixels (73.7%) have been classified into the three classes grouped as **P**. The common features of these pixels are small values of δ, s, and a. The major discriminant between the three **P** classes is the value of an average elevation. The class **P1** (21% of pixels) is the high elevation plateau, the class **P2** (32%) is the medium elevation plateau, and the class **P3** (20.7%) is the low elevation plateau.

The second largest group of pixels (18.5%) have been classified into four classes grouped as **C**. The common features of these pixels are large values of δ and $s_f = 0$. The major discriminant between the four **C** classes are the amount of flooding and the values of the slope. The class **C1** (2.8% of pixels) are pixels located on crater floor in deep craters. The class **C2** (7.8%) are pixels located on crater floor in medium-depth craters. The class **C3** (2.7%) are pixels located on craters walls. The class **C4** (5.2%) are pixels located in shallow, partially buried craters.

The ridges (7.4%) consist of two classes grouped as **R**. The common features of these pixels are large values of s, very small values of a, and $\delta = 0$. The class **R1** (2.7%) are pixels constituting craters rims. The class **R2** (4.7%) are pixels located at valley ridges, as well as on the outside slopes of craters. Finally, the class **CH** (0.4%) groups pixels characterized by large values of a. These pixels are the part of the landscape that constitutes the major drainage system. They could correspond to channels.

V. Statistical Analysis

A thematic map exhibits information in a style that differs from more familiar presentations like, for example, a topographic map (compare Fig. 2B. to Fig. 2A.). Visually, a thematic map appears simpler and easier to interpret than a topographic map. This is because a process of assigning meaning to the raw data has been automated by the pixel classification scheme. A thematic map offers pre-processed information. For example, on Fig. 2B., class **C4** represents "shallow craters" regardless of the elevation of their location. Notwithstanding the visual appeal of the resultant thematic map, the biggest advantage of our classification scheme is its semantic annotation of all pixels in the DTM.

Automatically generated thematic map, $\mathcal{M}(x, y)$ assigns semantic labels to the pixels. Adding $\mathcal{M}(x, y)$ to the $\mathcal{T}(x, y)$ as an extra layer produces a data structure that is ideal for statistical analysis of landscapes. This additional layer serves as a filter or a mask to isolate particular features for characterization and/ or comparison based on statistics of their constituent pixels.

To illustrate this point we have carried out a comparison of three plateau classes, **P1**, **P2**, and **P3** based on statistical analysis of properties of their constituent pixels. Specifically, we compare probability distribution functions (hereafter referred to as distributions and denoted by p) of a given variable constructed for different classes. The distributions of elevations for the three plateau classes are not overlapping, thus an elevation is a variable that discriminates between them. However, the distributions of δ, s, s_f, and a in the three plateau classes are almost identical. This confirms that all three classes pertain to the same type of terrain, an inter-crater plane, and differ only by an elevation.

Using pixels statistics we compare the floors of the two largest craters labeled "crater A" and "crater B" on Fig. 2B. In comparing the floors of these craters, we use craters locations, as well as $\mathcal{M}(x, y)$ as masks for selecting pixels of interest.

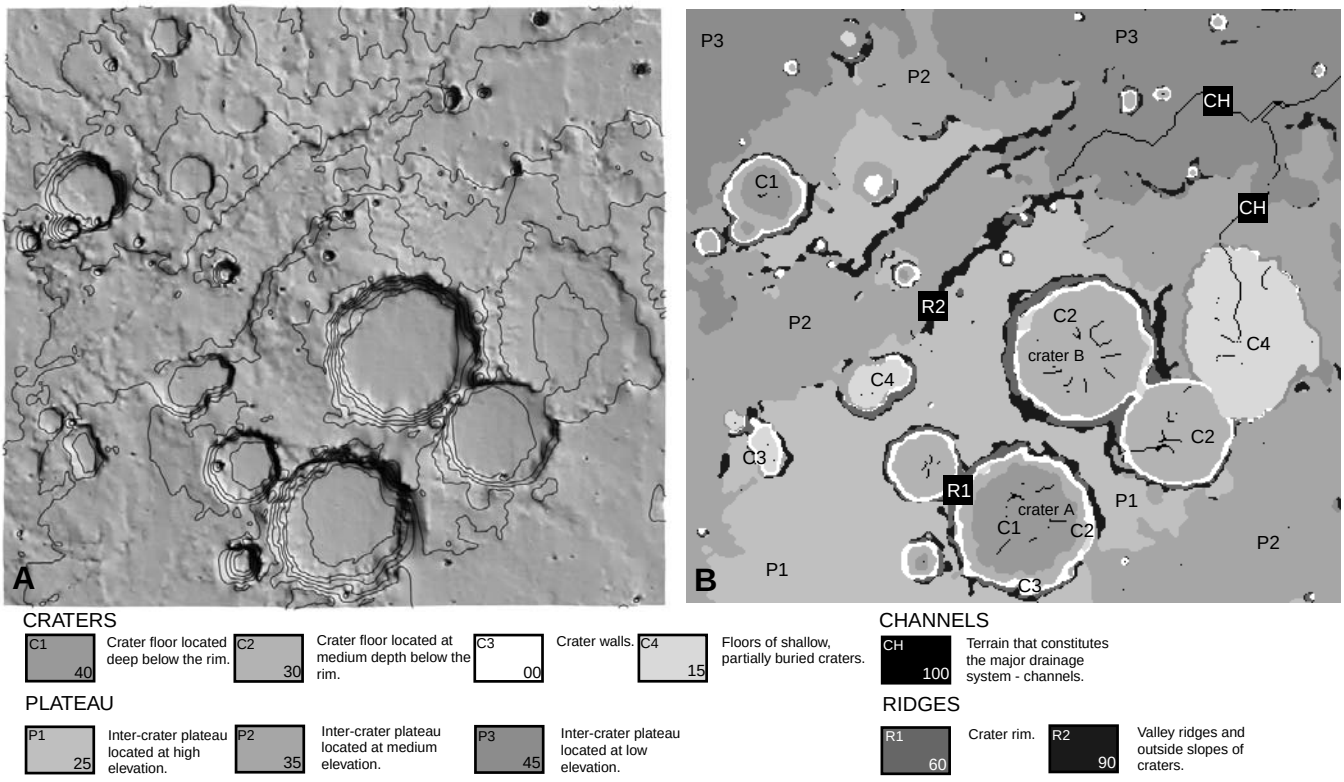

Fig. 2. **A.** Topographic contours superimposed on a shaded relief of Tisia Valles region on Mars. **B.** Thematic map of topography for Tisia Valles region constructed from classification of pixels in the DTM. Pixels belonging to the same class are indicated by the same shade of gray. The legend on the bottom ascribes physical meaning to the classes. The symbol in the upper-left corner of a shade-coding rectangle is the class label. The number in the lower-right corner of the rectangle is the percentage of gray level.

Population A consists of **C1** and **C2** pixels constituting the floor of crater A. Population B consists of **C2** pixels constituting the floor of crater B. Distributions of elevation, $p_{\rm A}(z)$ and $p_{\rm B}(z)$ have similar shapes indicating relative flatness of the floors in both craters. However, $p_{\rm B}(z)$ is shifted ~ 100 meters towards the higher elevations. Distributions of flooding adjustment, $p_{\rm A}(\delta)$ and $p_{\rm B}(\delta)$, have also similar shapes, but $p_{\rm B}(\delta)$ is shifted ~ 250 meters towards the lower values of δ. That means that the crater A is ~ 250 meters deeper than the crater B. Its floor is located at the lower elevation not because the crater is located at lower terrain, but because it is deeper. Distributions of slopes, $p_{\rm A}(s)$ and $p_{\rm B}(s)$ are almost identical. They are skewed toward small slopes confirming the relative flatness of floors in both craters.

Finally, it is interesting to compare statistics of classes **C3**, **R1**, and **R2** to characterize craters. We have constructed the distributions of elevations and slopes for pixels in these classes located in and around the crater A. Distributions $p_{\rm R1}(z)$ and $p_{\rm R2}(z)$ have similar shapes and ranges indicating that the rim of the crater is not elevated above its surroundings. The $p_{\rm C3}(z)$ has a different shape and is not overlapping with the other two distributions, reflecting the inside-the-crater location of the crater wall. Distributions $p_{\rm C3}(s)$ and $p_{\rm R1}(s)$ have very similar shapes, but $p_{\rm C3}(s)$ extends to the lower values of s. This indicates that crater's rim (as defined here) is an extension of its walls located at elevations above the lowest pour point of a crater (see Section II). The $p_{\rm R2}(s)$ has a different shape and it spans lower values of s pointing to a clear morphologic distinction between terrain located inside and outside of the crater. We have obtained the same results studying statistics of pixels in and around the crater B.

VI. Conclusion and Discussion

In this paper we have demonstrated a methodology for an automated and unsupervised classification of topographical features in Martian landscapes. It differs from similar methods applied in terrestrial context by using different topographic attributes and by relying on a different type of clustering algorithm. We have shown that our method is able to produce a thematic map of topography that serves as the first approximation to a geomorphic map. A side-by-side comparison of such a map and the topographic map (Fig. 2) reveals that our method has correctly identified all pertinent landforms. We have also demonstrated the usage of pixel statistics for quantitative characterization and comparison of different geomorphic features.

Our method yields high spatial integrity of the resultant topographic classes (see Fig. 2B.). Such integrity is desirable for any landform classification because topographical features are, after all, spatially coherent structures. Interestingly, our pixel-level classification produces high spatial coherence despite lack of any direct information about spatial relations between pixels. Achieving such coherence has been an issue in an automated classification of terrestrial landforms and additional

techniques, such as contextual merging [12] or fuzzy set classification [6], [13], have been proposed to improve it. We attribute the high spatial integrity of classes identified by our method to the inclusion of δ, a, and a_f into the DTM, topographic attributes not usually used in classification of terrestrial landforms. These attributes help to identify topographical basins (for example, craters) that are common and important features on Mars but occur rarely on Earth. Despite being assigned at-a-pixel, they represent a regional information (see Section II) and provide a connection between a local and a global scale.

Conceivably, there are other variables, relevant to both Martian and terrestrial landscapes, that help enforce the spatial integrity of topographic classes. For example, any variable obtained by integrating information from a sliding window wrapped around a pixel would have such property. In particular, our future studies will focus on two such variables, regional surface roughness and regional coherence of slope directions.

The regional surface roughness is calculated from the elevation field. It relates to a scatter of local elevations within a given region and can be quantified using the interquartile scale [14]. This quantity, denoted by $r_q(x,y)$, is a normalized distance between the first and the third quartile in a distribution of elevations collected from a square-shaped window wrapped around a pixel located at (x,y). Because distributions of elevations are typically long-tailed, r_q is more robust estimator of roughness than, say, the standard deviation [15].

Similarly, we can define coherence, $c(x,y)$, of regional local slope directions. Because of discretization, there are only eight possible slope directions. We collect values of slope directions from all pixels in a square window centered at (x,y). Next, the slope directions are re-labeled, the most abundant directions are labeled "1", the next most abundant directions are labeled "2" etc. We measure $c(x,y)$ as a standard deviation of a distribution of re-labeled slope directions. A small value of $c(x,y)$ indicates that slope directions within a neighborhood of (x,y) are preferentially aligned in the same direction. A large value of $c(x,y)$ signals lack of any preference in slope direction within a neighborhood of (x,y).

Both, $r_q(x,y)$ and $c(x,y)$ would be important additions to the DTM from the point of view of studying planetary surfaces, as well as studying terrestrial surfaces. In the terrestrial context yet more variables are conceivable. For example, following [16] we can include the field $l(x,y)$ of hillslope-to-channel length. The length $l(x,y)$ is the distance from a pixel at (x,y) to the nearest channeled pixel following the steepest descent path downslope. It is a scalar field that generalizes the traditional definition of globally defined drainage density. Finally, the concept of a DTM can be further extended to include layers of non-topographical information. For example, in a geological context, a multispectral image carrying remotely collected mineralogical information can be appended to the DTM carrying topographical information. The classification of the combined digital topography/spectra model would group pixels corresponding to specific topographic formations having similar mineral composition. In the context of Mars, the Thermal Emission Imaging System (THEMIS) instrument aboard Mars Odyssey Orbiter takes multispectral images of Martian surface. Once global mosaic of THEMIS images are produced [17] and referenced to the MOLA mosaic, it would become practical to append Martian DTM with spectral information.

ACKNOWLEDGMENT

This research was supported by NSF under grants IIS-0430208 and IIS-0431130. A portion of this research was conducted at the Lunar and Planetary Institute, which is operated by the USRA under contract CAN-NCC5-679 with NASA. This is LPI Contribution No. 1228.

REFERENCES

[1] D. E. Wilhelms, "Geologic Mapping", In *Planetary Mapping*, (R. Greeley and R. Batson, Eds.), Cambridge, UK: Cambridge Univ. Press, pp. 209-260, 1990.

[2] M. T. Zuber, D. E. Smith, S. C. Solomon, D. O. Muhleman, J. W. Head, J. B. Garvin, J. B. Abshire, and J. L. Bufton, "The Mars Observer Laser Altimeter Investigation", *J. Geophys. Res.*, vol. 97, no. E5, pp. 7781-7797, 1992.

[3] D. Smith, G. Neumann, R.E. Arvidson, E.A. Guinness, and S. Slavney, "Mars Global Surveyor Laser Altimeter Mission Experiment Gridded Data Record", *NASA Planetary Data System*, MGS-M-MOLA-5-MEGDR-L3-V1.0, 2003.

[4] J. R. Dymond, R. C. De Rose, and G.R. Harmsworth, "Automated Mapping of Land Components from Digital Elevation Data", *Earth Surface Processes and Landforms*, vol 20, pp. 131-137, 1995.

[5] F. Guzzetti and P. Reichenbach, "Towards a Definition of Topographic Divisions for Italy", *Geomorphology*, vol 11, pp. 57-74, 1994.

[6] B. J. Irvin, S. J. Ventura, and B. K. Slater "Fuzzy and Isodata Classification of Landform Elements from Digital Terrain Data in Pleasant Valley, Wisconsin", *Geoderma*, vol 77, pp. 137-154, 1997.

[7] D. Landgrebe, "The Evolution of Landsat Data Analysis", *Photogrammetric Engineering and Remote Sensing*, vol. LXIII, no. 7, pp. 859-867, 1997.

[8] D. G. Tarboton, R.L. Bras, and I. Rodriguez-Iturbe, "The analysis of river basins and channel networks using digital terrain data", *Technical Report* no. 326, Ralf M. Parsons Lab., MIT, Cambridge, 1989. (the software is available at www.engineering.usu.edu/dtarb/).

[9] G. McLachlan and T. Krishnan, *The EM Algorithm and Extensions.* New York, NY: John Wiley & Sons, 1997.

[10] P. Cheesman and J. Stutz, "Bayesian Classification (AutoClass) Theory and Practice", In *Advances in Knowledge Discovery and Data Mining*, (U. M. Fayyad, G. Piatetsky-Shapiro, P. Smyth and R. Uthurusamy, Eds.), MIT Press, pp. 153-180, 1996.

[11] J. R. Quinlan, *C4.5: Program for Machine Learning*, San Mateo, CA: Morgan Kaufmann, 1993.

[12] B. Romstad, "Improving Relief Classification with Contextual Merging", In *Proceedings of the 8th Scandinavian Research Conference on Geographical Information Science*, (J. T. Bjørke and H. Tveide, Eds), Ås, Norway, pp. 3-14, 2001.

[13] P. A. Burrough, P. F. M. van Gaans, and R. A. MacMillan, "High-resolution Landform Classification Using Fuzzy k-Means", *Fuzzy Sets and Systems*, vol. 113, pp. 37-52, 2000.

[14] G. A. Neumann and D. W. Forsyth, "High Resolution Statistical Estimation of Seafloor Morphology", *Marine Geophys. Res.*, vol. 17, pp. 221-250, 1995.

[15] O. Aharonson, M. T. Zuber, and G. A. Neumann, "Mars: Northen hemisphere slopes and slope distributions", *Geophys. Res. Lett.*, vol. 25, pp. 4413-4416, 1998.

[16] G. E. Tucker, F. Catani, A. Rinaldo, and R. L. Bras, "Statistical analysis of drainage density from digital terrain data", *Geomorphology*, vol. 36, pp. 187-202, 2001.

[17] B. A. Archinal, L. Weller, S. Sides, G. Cushing, R. L. Kirk, A. Soderblom, and T. C. Duxbury, "Preparing for Themis Controlled Global Mars Mosaic", In *Lunar and Planetary Science XXXV*, #1903, Lunar and Planetary Institute, Houston (CD-ROM), 2004.